ACS APPLIED MATERIALS & INTERFACES

Research Article

www.acsami.org

Adsorption of Arginine–Glycine–Aspartate Tripeptide onto Negatively Charged Rutile (110) Mediated by Cations: The Effect of Surface Hydroxylation

Chunya Wu,*[,†] Mingjun Chen,*[,†] Adam A. Skelton,[‡] Peter T. Cummings,[§,∥] and Ting Zheng[†]

[†]Center for Precision Engineering, Harbin Institute of Technology, P.O. Box 413, Harbin, Heilongjiang 150001, China

[‡]Department of Chemical & Material Engineering, University of Dayton, 300 College Park, Dayton, Ohio 45469, United States

[§]Department of Chemical & Biomolecular Engineering, Vanderbilt University, Nashville, Tennessee 37235-1604, United States

[∥]Center for Nanophase Materials Sciences, Oak Ridge National Laboratory, Oak Ridge, Tennessee 37831-6494, United States

Supporting Information

ABSTRACT: Classical molecular dynamics (MD) simulations were employed to investigate the adsorption behaviors of arginine–glycine–aspartate (RGD) tripeptide onto the negatively charged hydroxylated/nonhydroxylated rutile (110) surfaces, mediated by biologically important cations (Na^+ or Ca^{2+}). The simulation results indicate that the inherent nature of the cation determines its binding strength, thereby regulating the adsorption geometry of the peptide. The sparse hydroxyl groups on the nonhydroxylated rutile diminish the probability of H-bond formation between RGD and the surface, resulting in an early desorption of the peptide even with a mediating Na^+ ion. In contrast, the negatively charged aspartate (Asp) side chain is bridged to the negatively charged hydroxylated rutile by an inner-sphere Na^+ ion, in coordination with the Asp–rutile hydrogen bonds at the anchoring sites. The inner- and outer-sphere Ca^{2+} ions are demonstrated to be capable of "trapping" RGD on both hydroxylated and nonhydroxylated rutile, in the absence of hydrogen bonds with the surface. The strongly bound inner-sphere mediating Ca^{2+} ion exerts a "gluing" effect on the Asp side chain, producing a tightly packed RGD–rutile complex, whereas a less localized distribution density of the outer-sphere mediating Ca^{2+} ion results in a higher mobility of the Asp side chain. The intramolecular interaction is suggested to facilitate the structural stability of RGD adsorbed on the negative rutile in a "horseshoe" configuration.

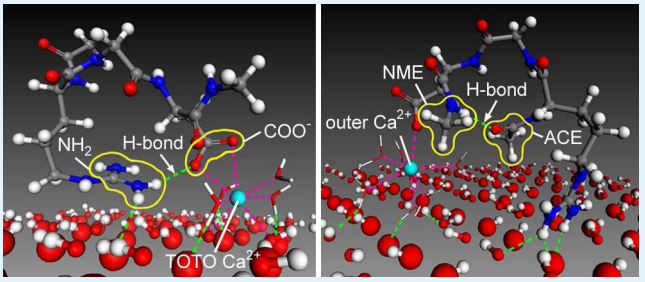

KEYWORDS: *RGD tripeptide, molecular dynamics simulation, cation mediation, binding configuration, intramolecular interaction, interaction energy*

INTRODUCTION

The research scope of interactions between the proteins and the surfaces of inorganic materials has been much broadened recently, due to its paramount importance in several natural processes.[1,2] For instance, when a bone-anchored implant is suddenly placed in a human body, the soluble proteins in blood serum will preferentially interact with the surface of the implant, saturating it within a time frame of seconds to minutes.[3] As a consequence, unwanted reactions may be induced with the biocompatibility of the implanted materials affected in a negative way.[4] A wealth of experimental and theoretical studies[5−8] have been devoted to devising an efficient way to improve the surface biocompatibility, which is especially required in implanted materials to accelerate tissue regeneration and growth. For now, a biomimetic approach based on the precoating of biological factors seems to be a feasible option to optimize the properties of implant surfaces,[9] thereby helping to recruit cells in the first step of implantation and consequently accelerate cell colonization and biointegration.[10] However, the covalent immobilization technique is relatively expensive and involved;[11] thus the strong, specific adsorption of proteins or other biomolecules (acting as a biotarget identifier) onto the surface of the implant seems to be a good alternative to emulating biology in the fabrication of materials.[12]

Integrins are heterodimeric cell surface receptors that were found to mediate cell–extracellular matrix (ECM) adhesion by binding to the ligands with an exposed arginine–glycine–aspartate (RGD) sequence.[13,14] This sequence is a ubiquitous adhesive motif in ECM proteins with a high affinity to the predominant osteoblast integrin;[15,16] thus many experiments[17−23] have been focused on exploring the use of RGD for the biomimic coating of bone–anchored implants, especially the widely used titanium–based materials. Ferris[17] and Rammelta[20] discovered that the immobilized RGD-coating

Received: December 18, 2012
Accepted: March 5, 2013
Published: March 5, 2013

could increase the bone remodeling activity around the titanium implants. Maddikeri et al.[22] found that RGD may be capable of preventing unspecific adhesion of cells on titanium, resulting in a selective biointeractive pattern. The experimental data obtained by Chen et al.[21] showed an accelerated bone growth into the Ti-6Al-4 V implant with the combination of microgrooving and RGD-coating, compared to the individual effects of these two factors. Although the effectiveness of the implanted RGD-functionalized titanium-based materials in enhancing bone healing has been demonstrated by experimental studies, the underlying reasons for it, e.g., adsorption mechanism of the peptide, are not yet quite clarified. As documented previously,[10] computational approaches, which can help to screen biomolecule−surface interactions and analyze the elementary events leading to adsorption, may be a very promising way to solve this problem.

Titanium−based materials are known to naturally have a thin but strongly adherent oxide layer (TiO_2).[24,25] Rutile is the most stable phase of TiO_2 polymorphs at ambient temperature,[26] thereby being widely used as the adsorbent in simulations.[27−33] Song et al.[27] revealed that the side chains of RGD were inclined to bind with the rutile by electrostatic and van der Waals interactions. Zhang et al.[28] found that water layers limited the RGD−rutile interaction, helping to sustain the initial configuration of the peptide. The results in our previous simulation studies[29,30] indicated that RGD bound to the reduced rutile surface (part of atoms in the top layer were removed) exhibited a higher adsorption energy than the peptide bound to the ideal, flat surface both in vacuum and aqueous solution. The efforts to computationally describe RGD−rutile interaction have shed some light on the key factors determining the behavior of peptide deposited on clean rutile surfaces, covering driving force, interfacial water layers, surface topography, etc. However, some aspects of the binding mechanism, e.g., the hydroxylation state, the charges of adsorbate and adsorbent, and the charge shielding of compensating ions, are still poorly understood at the molecular level, whereas the importance of these factors in protein adsorption has been highlighted in experimental studies.[34−39] Feng et al.[34] found that the adsorption of bovine serum albumin on TiO_2 was positively correlated with the amounts of surface hydroxyl groups. The charged end group of the peptide was known to be attracted to the oppositely charged adsorbent surface;[40−42] however, a phenomenon that a positively charged protein adsorbed onto a positively charged interface was also observed by Lesins and Ruckenstein.[35] This was attributed to the distribution of amino acid residues on the protein surface, which resulted in patches of negative charge, opposite to the net positive charge of the surface, as suggested in other experiments.[36−38] The observation gained by Dishon et al.[43] is a typical illustration of charge shielding. More cations adsorbed to the negatively charged surface as salt concentration increased, gradually neutralizing the surface charge and, hence, suppressing the electrostatic double layer repulsion, revealing van der Waals attraction. At even higher salt concentrations, repulsion re-emerged due to surface charge reversal by the excess of adsorbed cations.

Considering the importance of hydroxylation state, surface charge, and compensating ions, it should be of interest to elucidate the interplay of these factors in peptide−surface interaction by means of classical molecular dynamics (MD) simulation. Since water is an integral part of the environment in most of the applications of Ti-materials, the hydroxyl coverage of a native oxide film formed on a Ti-surface depends on the adsorption state of water. However, the fundamental question that whether the water dissociates upon adsorption on the TiO_2 surface has not reached a consensus between experimentalists and theorists. Among the experimental studies, the common view is that at all coverages water adsorbs molecularly on the ideal TiO_2 (110) surface and dissociation does only take place at defect sites,[44−48] whereas early theoretical calculations predicted water dissociation at all coverages.[49,50] Recently, a delicate balance between dissociated, partial dissociated, and molecular adsorption of water has been suggested in both experimental and theoretical studies.[51−53] Walle et al.[51] presented evidence for mixed molecular and dissociative water adsorption at monolayer coverage on a defect-free rutile TiO_2 (110) surface using synchrotron radiation photoemission, in agreement with the theoretical prediction proposed by Lindan and Zhang[52] that a mixed molecular-dissociated configuration was the most stable adsorption state of water. Lindan and Zhang[52] suggested that the dissociation of water at low coverages was not observed experimentally because of the hindrance from a significant dissociation barrier which was difficult to overcome on the time scale of the experiments. However, Kowalski et al.[54] believed that whether the dissociation of water molecules at low coverage was prevented by a large dissociation barrier cannot be confirmed on the basis of their DFT calculation results. Since available experimental and theoretical results cannot give a clear-cut answer to whether water adsorbs associatively or there is dissociation of water to produce hydroxyl sites on the TiO_2 (110) surface, a compromise was offered in this paper. That is, two extreme cases of rutile (110) surface, characterized by a different degree of hydroxylation with a charge density of -0.208 C/m^2 (corresponding to pH ∼7.80)[55] were presented to test both the hydroxylated and nonhydroxylated state of the surface, attempting to figure out a way to better approximate the real surface. One case is a surface with a full coverage of terminal hydroxyls (TOH, binding to a 5-fold coordinated surface titanium, Ti_5) and a smaller coverage of bridging hydroxyls (BOH, formed by adding a hydrogen atom to a doubly coordinated bridging oxygen; 75% coverage), while the other extreme case is a surface with a selected number of TOHs (25% coverage) but no BOH. Taking into account the similarity of these surfaces to the neutral hydroxylated/nonhydroxylated rutile, we termed the above two surfaces the *negative hydroxylated surface* (the former, hereafter called "hyd-surface:) and the *negative nonhydroxylated surface* (the latter, hereafter called "nonh-surface"), respectively.

The role of mediating cations in determining the binding geometry of the negatively charged aspartate residue (Asp) to the negatively charged hyd-surface has been investigated previously.[56] The doubly charged cations (Mg^{2+}, Ca^{2+}, Sr^{2+}) were found to mediate the Asp residue more strongly than the singly charged cations (K^+, Na^+, Rb^+) on the hyd-surface. Since the difference between the hyd- and nonh-surfaces results in different degrees of coverage of the available adsorption sites,[57] it should be considered that the binding configuration of cations may be affected, thereby probably exercising a different influence on the mediating activity. In the present study, we intend to test the dependence of RGD−rutile interaction on the local microenvironment, including the coverage of hydroxyl groups, the species of compensating ions (Na^+ and Ca^{2+}), and their binding modes. The simulation results referring to the nonh-surface will be discussed in detail, whereas for the hyd-

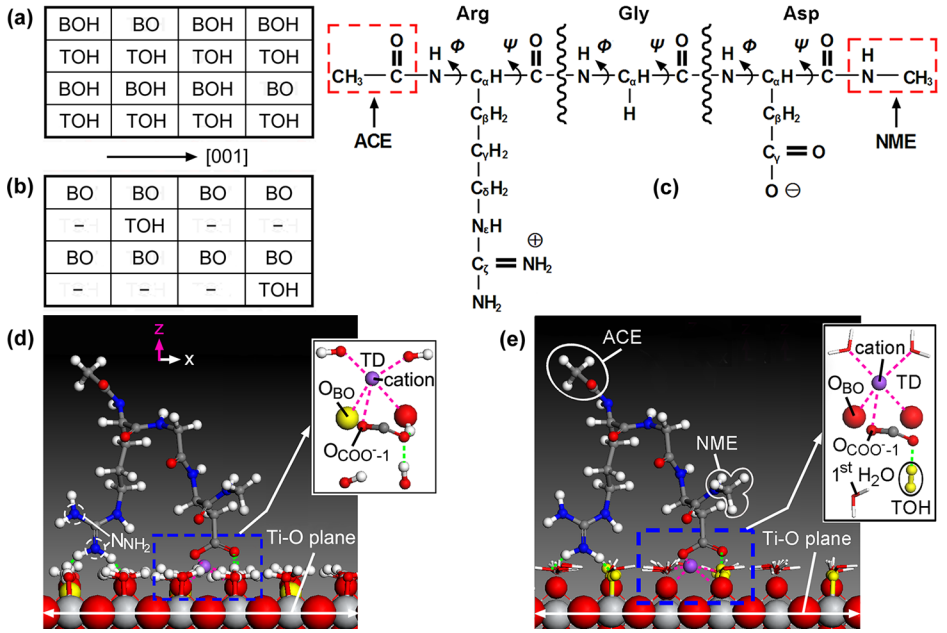

Figure 1. (a) Geometric scheme of the distribution of surface groups on the negatively charged hydroxylated rutile (110) (hyd-surface). (b) Geometric scheme of the distribution of surface groups on the negatively charged nonhydroxylated rutile (110) (nonh-surface). (c) Structure of RGD tripeptide. (d) Initial configuration of RGD on the hyd-surface. (e) Initial configuration of RGD on the nonh-surface. The insets show the COO^-–surface binding sites on the two surfaces.

surface, only the aspects not included previously will be mentioned. A direct comparison between the adsorption propensities of RGD on the hyd- and nonh-surfaces will, therefore, be made.

SIMULATION METHODS

The elementary structure of rutile (110) cell (l_x = 5.918 Å, l_y = 6.497 Å) was obtained from ab initio calculations.[58] The geometric distributions of surface groups for the hyd- and nonh-surfaces shown in Figure 1a and b were proposed and tested by Předota.[58] Since the structure of the entire surface was a periodic replication of the unit displayed in Figure 1a or b, the adopted distribution pattern keeps the separation of each BO group on the hyd-surface (or TOH group on the nonh-surface) from its nearest neighboring BO group (or TOH group on the nonh-surface) maximum and uniform, thus minimizing Coulombic repulsion. On the nonh-surface, 75% of the Ti_5 atoms were originally bare (indicated by "–"); thus, water molecules in the bulk approached the surface and coordinated to the bare Ti_5 atoms, thereby being called "1st H_2O" in the following. The RGD sequence (shown in Figure 1c) with a configuration reminiscent of the "horseshoe" structure[59] on the presented rutile surfaces was immersed in NaCl and $CaCl_2$ solutions, respectively. The side chains of arginine (Arg, pK_a = 12.0) and Asp (pK_a = 3.90) were considered to be ionized at pH ~7.80, thus carrying a net positive charge and a net negative charge, respectively. The termini of RGD were blocked with ACE and NME groups to mimic a peptide bond to account for the continuation of the sequence. As shown in the insets, the COO^- group on the hyd-surface was positioned close to a deprotonated O_{BO}, forming two hydrogen bonds with the neighboring BOH and TOH groups (Figure 1d), while the COO^- group on the nonh-surface was initially H-bonded to a TOH group (Figure 1e). For both surfaces, a cation (Na^+ or Ca^{2+}) was placed in the vicinity of the COO^- group to mediate the RGD/rutile binding. Up to 2194 water molecules were added, filling the simulation box of approximate size 47 Å × 52 Å × 50 Å. Ions with a proportion of 48 Na^+/16 Cl^- or 24 Ca^{2+}/16 Cl^- were dissolved in the aqueous solution to compensate the total negative structural charge of −32e of the rutile (110) surfaces.

MD simulations of the RGD/rutile/aqueous solution system were performed in the NVT ensemble by using the LAMMPS package.[60] The AMBER force field[61] was adopted to describe the peptide structures. The SPC/E model was used to represent the water molecules.[62] The parameters of Lennard-Jones potential for the cross interactions between nonbonded atoms were obtained from the Lorentz–Berthelot rule.[63] The rutile parameters and the interaction potentials between the rutile atoms and the peptide/water atoms were obtained from the literature.[58,64] The details of potential parameters and the validation of the adopted force fields by other researchers were summarized in the Supporting Information. Periodic boundary conditions were applied in the *x*- and *y*-direction, and a reflecting boundary condition was applied in the *z*-direction.

Surface atoms on and below the Ti–O plane (see Figure 1d and 1e) were frozen during the entire simulation, while the surface atoms above the Ti–O plane (i.e., TOH, BOH, and O_{BO}) were kept flexible; however, the Ti–O bonds (hyd-surface: for O_{TOH} and O_{BO}; nonh-surface: for O_{TOH}) and O–H bonds (for TOH and BOH) were constrained using the Shake algorithm. At the beginning, RGD was held rigid in the initial coordinates to randomize the position of the solvent (water and ions) without disrupting the "horseshoe" configuration. After an energy minimization (corresponding to a 0 K MD simulation), solute constraints were removed and the system was heated under constant volume to 300 K in steps of 50 K before commencing the production run at 310 K. The production MD simulation was conducted for 6 ns in the NVT ensemble, with the first 4 ns considered equilibration and the final 2 ns used for statistical analysis.

RESULTS AND DISCUSSION

Cations at the Rutile/Water Interface. The adsorption propensities of Na^+ and Ca^{2+} ions on the hyd- and nonh-surfaces were initially examined to find out the effect of compensating ions on the RGD–rutile interaction; thus the inner-sphere and outer-sphere concepts should be introduced first to characterize the adsorption mode of ions. An ion in the outer-sphere mode is adsorbed at the surface through its solvation shell, whereas in the inner-sphere adsorption mode, one (or more) surface hydroxyl(s) (including 1st H_2O on the nonh-surface) substitute one (or more) water molecule(s) from

dx.doi.org/10.1021/am3031568 | ACS Appl. Mater. Interfaces 2013, 5, 2567–2579

the solvation shell of the ion.[10] The axial densities of cations (the number of ions per cubic angstrom) are displayed in Figure 2, where the zero point of the horizontal axis (i.e., $z = 0$)

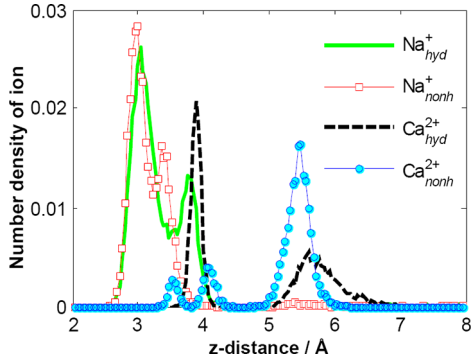

Figure 2. Axial density profile of Na^+ and Ca^{2+} ions on the hyd- and nonh-surfaces.

was defined as the position that the surface layer of Ti atoms would occupy in the unrelaxed crystal termination (the definition is identical for the presented two surfaces) and will hereafter be called "rutile plane". The adsorbed Na^+ ions on both surfaces keep close to the rutile plane (z < 4.2 Å), indicating that Na^+ ions in the bulk phase can readily escape from the coordination shell of water molecules to bind directly to the surface in an inner-sphere configuration. The axial density profile of Ca^{2+} ions on the hyd-surface is characterized by two comparable peaks, i.e., equal amounts of inner- and outer-sphere adsorbed Ca^{2+} ions, whereas the axial density profile of Ca^{2+} ions on the nonh-surface exhibits three peaks with the height of the third peak (centering at ~5.45 Å) far greater than the first two, showing an overwhelming majority of the outer-sphere binding configuration. To better understand the binding mechanism of cations at the water/rutile interface, the heights of the adsorbed cations and the occupancies of the available binding modes (the percentage of cations in a given adsorption site relative to the total number of cations in the region 0–7 Å from the rutile plane) were listed in Table 1.

The inner-sphere binding sites on hyd- and nonh-surfaces are composed of two bidentate sites, i.e., BD-BOTO and BD-TOTO (BO refers to the bridging oxygens, including protonated O_{BOH} and deprotoned O_{BO}; TO refers to the terminal oxygens, including O_{TOH} and oxygens of the 1st H_2O: 1st O_W), and a tetradentate site (TD) formed by two terminal oxygens and two bridging oxygens. As seen from Table 1, the adsorbed TD and BD-BOTO Na^+ ions on the hyd-surface locate a little higher than that on the nonh-surface, whereas the case for the BD-TOTO Na^+ and BD-TOTO Ca^{2+} is opposite. This probably arises from the differences in the heights of atoms constituting the binding sites; thus, the axial density profiles of surface oxygen atoms and water oxygen atoms, obtained from the surfaces immersed in NaCl solution, were plotted in Figure 3 with the data listed in Table 2. The peaks

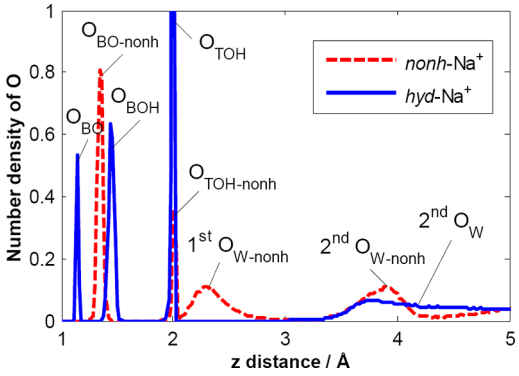

Figure 3. Axial density profile of oxygen atoms.

Table 2. Heights of Surface Oxygen Atoms (Including 1st and 2nd Water Oxygens)[a]

atom	hyd-surface	nonh-surface
O_{BO}	1.14 ± 0.02 (1.13 ± 0.05)	1.34 ± 0.06 (1.25 ± 0.05)
O_{BOH}	1.44 ± 0.05 (1.36 ± 0.05)	
O_{TOH}	1.98 ± 0.03 (1.97 ± 0.05)	2.00 ± 0.04 (2.00 ± 0.05)
1st O_W		2.34 ± 0.20 (2.37 ± 0.10)
2nd O_W	3.96 ± 0.36	3.76 ± 0.28

[a]Quantities in parentheses are from ref 58.

for the nonh-surface in Figure 3 are denoted by the subscript "nonh", while the ones without any special denotation refer to the hyd-surface. The values listed in Table 2 are consistent with a previous simulation work[58] (quantities in parentheses), except the O_{BOH} on the hyd-surface and the O_{BO} on the nonh-surface ($O_{BO\text{-}nonh}$) because neither the Ti–O_{BOH} bonds nor the Ti–$O_{BO\text{-}nonh}$ bonds were constrained during the simulation. If we apply constraints to the above two types of bonds, the shake clusters (i.e., Ti–O_{BOH}–Ti or Ti–$O_{BO\text{-}nonh}$–Ti) will be connected at one Ti atom. Since LAMMPS is not currently capable of handling such a constraint, the bonds between the O_{BOH} (or $O_{BO\text{-}nonh}$) and Ti atoms were kept flexible with an appropriate force constant. The results do not differ significantly from the simulation with fixed bonds.

The O_{BO} atoms on the nonh-surface are lower than the O_{BOH} atoms on the hyd-surface (1.34 vs 1.44, Table 2); therefore, the cations in the binding modes of TD and BD-BOTO locate

Table 1. Binding Configurations, Occupancies, and Heights of Cations on the Negatively Charged Hydroxylated/Nonhydroxylated Rutile (110) Surface

	inner-sphere							
	TD		BD-BOTO[a]		BD-TOTO[a]		outer-sphere	
ion	h/Å	occup/%	h/Å	occup/%	h/Å	occup/%	h/Å	occup/%
hyd-Na^+	3.04	57.61	3.49	12.71	3.78	27.42	5.86	2.26
nonh-Na^+	3.00	67.30	3.44	28.30	3.84	3.15	5.58	1.25
hyd-Ca^{2+}		0		0	3.87	49.91	5.76	50.09
nonh-Ca^{2+}		0	3.53	5.89	4.08	11.79	5.44	82.32

[a]TO refers to the terminal oxygens, including O_{TOH} and 1st O_W. BO refers to the bridging oxygens, including O_{BOH} and O_{BO}.

dx.doi.org/10.1021/am3031568 | ACS Appl. Mater. Interfaces 2013, 5, 2567–2579

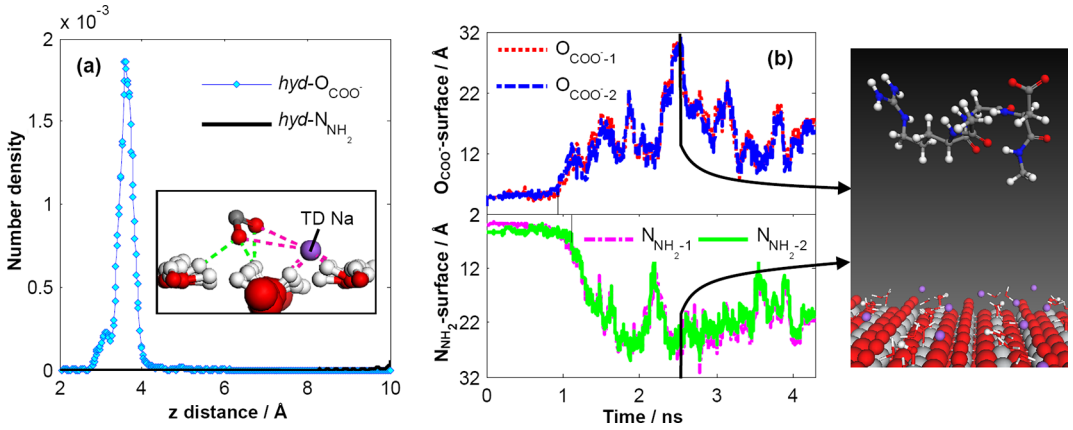

Figure 4. (a) Axial density of functional atoms on the hyd-surface in NaCl solution. (b) Evolution of *z*-distances from the O_{COO^-} and N_{NH2} atoms to the rutile plane for the nonh-surface. The inset shows the configuration of RGD after desorption from the surface.

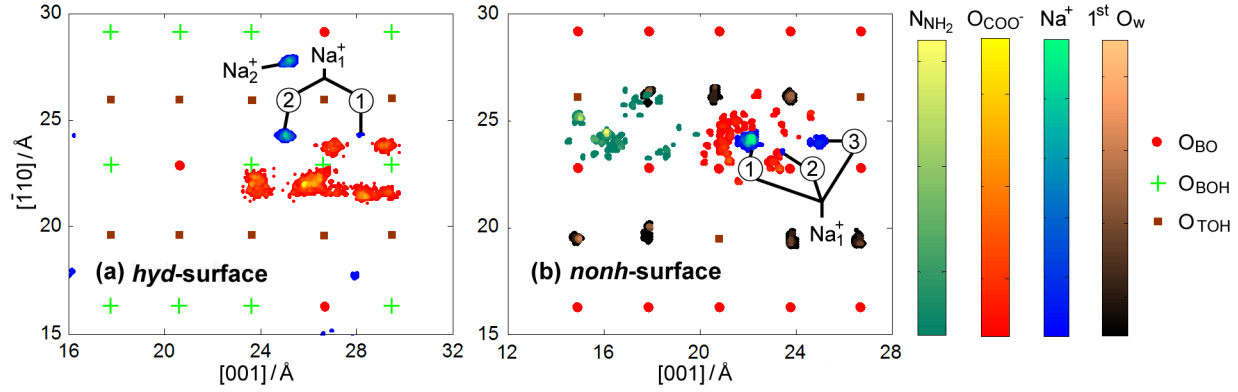

Figure 5. 2D density maps of functional atoms in NaCl solution: (a) hyd-surface; (b) nonh-surface.

closer to the nonh-surface than the hyd-surface. The heights of O_{TOH} atoms are almost identical for both hyd- and nonh-surfaces; however, the 1st O_W atoms on the nonh-surface stay much higher than the O_{TOH} atoms (2.34 vs 1.98, Table 2). This explains why the BD-TOTO cations are pushed much farther away from the nonh-surface than the hyd-surface (the BD-TOTO binding sites on the nonh-surface are formed by two 1st O_W atoms or one O_{TOH} and one 1st O_W). The outer-sphere Ca^{2+} ions bind to the hyd- and nonh-surfaces indirectly, via the mediation of the second water layer, but the height of these cations from the hyd-surface is much greater than the height from the nonh-surface (5.76 vs 5.44, Table 1). This difference arises from the difference in the average height of water oxygen atoms of the second layer (hyd-surface 3.96 Å; nonh-surface 3.76 Å, Table 2). Considering the significant proportion of outer-sphere Ca^{2+} ions on the presented surfaces, their mediating strength in RGD−rutile interaction should be investigated in detail to compare with the inner-sphere Ca^{2+} ions. Also, the mediation of TD Na^+ ions on both hyd- and nonh-surfaces will be discussed because of the predominance of this binding geometry in the adsorbed Na^+ ions.

RGD−Rutile Binding Mediated by Cations. Many experimental studies have confirmed that the electrostatic double-layer repulsion between the negatively charged adsorbate and the like-charged adsorbent can be overcome by cation shielding.[65−67] Since it has been shown above that the properties of adsorbed cations on the hyd- and nonh-surfaces differ, it should be considered whether the difference in the binding properties of cations on different surfaces will in turn affect their mediation between the peptide and the surface. In the presented systems, the peptide exhibits a horseshoe configuration with both positively charged Arg and negatively charged Asp side chains initially attached to the surface. The desorption of either side chain will result in the collapse of the horseshoe configuration; thus the mobility of Arg and Asp side chains will be the focus of analysis in the following to examine the structural change of the peptide within the time scale of the simulation. The axial densities of atoms in the functional groups, i.e., oxygens in the COO^- group (O_{COO^-}) and nitrogens in the NH_2 groups (N_{NH_2}, labeled in Figure 1d) will be reported first. The threshold to classify the O_{COO^-} or N_{NH_2} atoms as being "on the surface" or not will be determined according to the position of the first/second minimum of the axial density profile (The values will be provided below). That is, if the *z*-distance of O_{COO^-} or N_{NH_2} atoms from the rutile plane is smaller than the threshold, the atoms will be regarded as being on the surface. The 2D density maps representing the planar positions of the O_{COO^-} and N_{NH_2} atoms on the surface will be adopted to visualize the binding sites of RGD. In addition, the distribution of backbone dihedrals will be considered to compare the conformational stability of RGD on the hyd- and nonh-surfaces. All the statistical data were averaged from the final 2 ns production run except special declaration.

Adsorption of RGD on the Negatively Charged Rutile Mediated by Na^+. This section will show the results of RGD adsorption on the negatively charged hydroxylated and

nonhydroxylated rutile (110) surfaces when immersed in NaCl solution. The hyd-surface, already described in our previous work[68] will be briefly discussed to compare with the results of the nonh-surface. The RGD peptides with the same horseshoe configuration were initially put close to the hyd- and nonh-surfaces, respectively. Figure 4 displays the axial density profiles of the functional atoms on the hyd-surface (Figure 4a), and the evolution of z-distances from the functional atoms to the rutile plane for the nonh-surface during the temperature rise stage and the first 4 ns of the production run (Figure 4b).

As seen from Figure 4a, the axial density of hyd-O_{COO^-} has a first sharp peak centered at ~3.60 Å, indicating that the COO^- group stays close to the hyd-surface (The predominant conformation of the COO^- group is shown in the inset of Figure 4a), whereas the Arg side chain detaches from the hyd-surface completely. The RGD on the nonh-surface behaves differently to the peptide on the hyd-surface. As shown in Figure 4b, the COO^- group stays on the nonh-surface only for a short time (less than 1 ns), even though a preadsorbed Na^+ ion was placed close to it at the beginning of the simulation (see the inset of Figure 1e). The NH_2 groups move into the bulk phase soon after the COO^- group comes off the nonh-surface. The snapshot of RGD after desorption is displayed in the inset of Figure 4b.

To visualize the positions of functional atoms in the $x-y$ plane, the 2D density maps of the O_{COO^-} and N_{NH_2} atoms on the surface (threshold: 6 Å for the O_{COO^-} and N_{NH_2} atoms), as well as the adsorbed cations are shown in Figure 5. Figure 5a shows the result for the hyd-surface during the final 2 ns production run, whereas Figure 5b gives the results for the nonh-surface during the first 1 ns of the time stage shown in Figure 4b, because the peptide sticks to the former surface during the entire production run, but detaches from the latter surface at the early stage of the simulation. On the basis of our previous work,[68] only additional discussions about the 2D density map will be presented for the hyd-surface.

The COO^- group on the hyd-surface remains in close proximity to the adjacent BOH groups, forming hydrogen bonds with the H_{BOH} (Figure 5a). However, the mediating Na^+ ion moves from position 1 to position 2 (labeled in Figure 5a) during the final 2 ns production run, whereas the migration of the COO^- group following the mediating Na^+ is hindered by the $H_{BOH}\cdots O_{COO^-}$ hydrogen bonds. After the mediating Na^+ ion is stabilized in position 2, the COO^- group moves along the [001] direction, keeping both O_{COO^-} atoms coordinated to this specific cation.

For the nonh-surface, less localized densities of the O_{COO^-} and N_{NH_2} atoms are presented, indicating that the COO^- and NH_2 groups stay on the surface with a high mobility during the first 1 ns of the simulation, when the preadsorbed Na^+ ion occupies three different positions (labeled in Figure 5b). This Na^+ ion stays in position 1 for ~0.8 ns with the coordinated COO^- group moving around it, meanwhile the O_{COO^-} atoms do not form stable hydrogen bonds with the sparse TOH groups or the 1st H_2O. The mediating Na^+ ion moves from position 1 to the temporary site, position 2, and then immediately moves to position 3. As a consequence, the direct bonds between the O_{COO^-} atoms and the preadsorbed Na^+ ion break completely at the end of the first 1 ns, which finally results in the desorption of the peptide. As discussed in our previous study, the bulk Na^+ ions with a loose hydration shell are readily desolvated (the residence time of first coordination shell of water molecules around Na^+ ion is less than 30 ps),[56] which suggests an inherent nature to the direct bonds connected with Na^+ ions. That is, the instability of direct bonds from the mediating Na^+ ion to the O_{COO^-} or surface oxygen atoms is similar to the case for the Na^+-O_W bonds, which break and reform frequently; therefore, it makes sense that the mediating Na^+ ion can move in the $x-y$ plane of the hyd- or nonh-surface, and leave/approach the COO^- group easily. On the hyd-surface, the $Na^+-O_{COO^-}$ direct bonds seem not to be permanent; however, the mediating Na^+ ion is actively involved in bridging the negatively charged COO^- group to the negatively charged hyd-surface during the entire simulation, in coordination with the $H_{BOH}\cdots O_{COO^-}$ hydrogen bonds at the anchoring sites. In contrast, the RGD desorbs from the nonh-surface at an early stage of the simulation even in the presence of a preadsorbed mediating Na^+, which mainly results from the sparsity of hydroxyl groups on the nonh-surface (the coverage of hydroxyl groups: BOH = 0, TOH = 25%). Since the probability of H-bond formation between the peptide and the surface is diminished significantly, the Asp side chain cannot be trapped on the nonh-surface solely by the mediation of a single Na^+ ion.

Adsorption of RGD on the Negatively Charged Rutile Mediated by Inner-Sphere Ca^+. To compare the ability of the doubly charged Ca^{2+} ion with the singly charged Na^+ ion in mediating RGD adsorption on the negatively charged rutile (110), the simulations of RGD−rutile (hyd-/nonh-surface) complex with a preadsorbed TD Ca^{2+} ion were conducted. For the sake of clarity, the items involved in these two systems will be denoted by "hyd_1-" and "$nonh_1$-", respectively. In the following analysis, new discussions about the mediation of inner-sphere Ca^{2+} ion on the hyd-surface will be added in order to directly compare with the results for the nonh-surface.

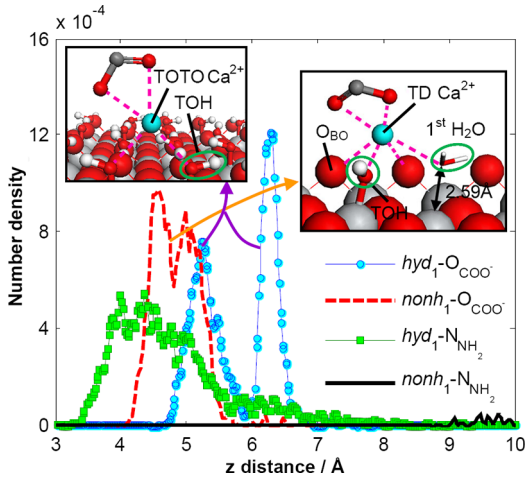

Figure 6. Axial density profile of functional atoms mediated by an inner-sphere Ca^{2+} ion on the hyd- and nonh-surfaces.

Figure 6 displays the axial density profiles of O_{COO^-} and N_{NH_2} atoms. The hyd_1-N_{NH_2} atoms distribute roughly within the range of 3−7 Å above the rutile plane, forming hydrogen bonds with the negatively charged hyd-surface, whereas the $nonh_1$-N_{NH_2} atoms stay farther away from the rutile plane (>9 Å). On the contrary, the axial densities of O_{COO^-} atoms on the hyd- and

dx.doi.org/10.1021/am3031568 | ACS Appl. Mater. Interfaces 2013, 5, 2567−2579

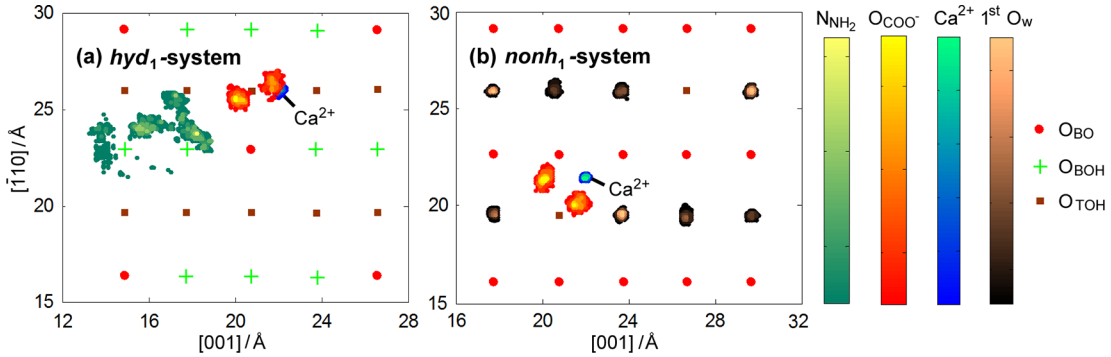

Figure 7. 2D density maps of functional atoms mediated by an inner-sphere Ca^{2+} ion: (a) hyd-surface, (b) nonh-surface.

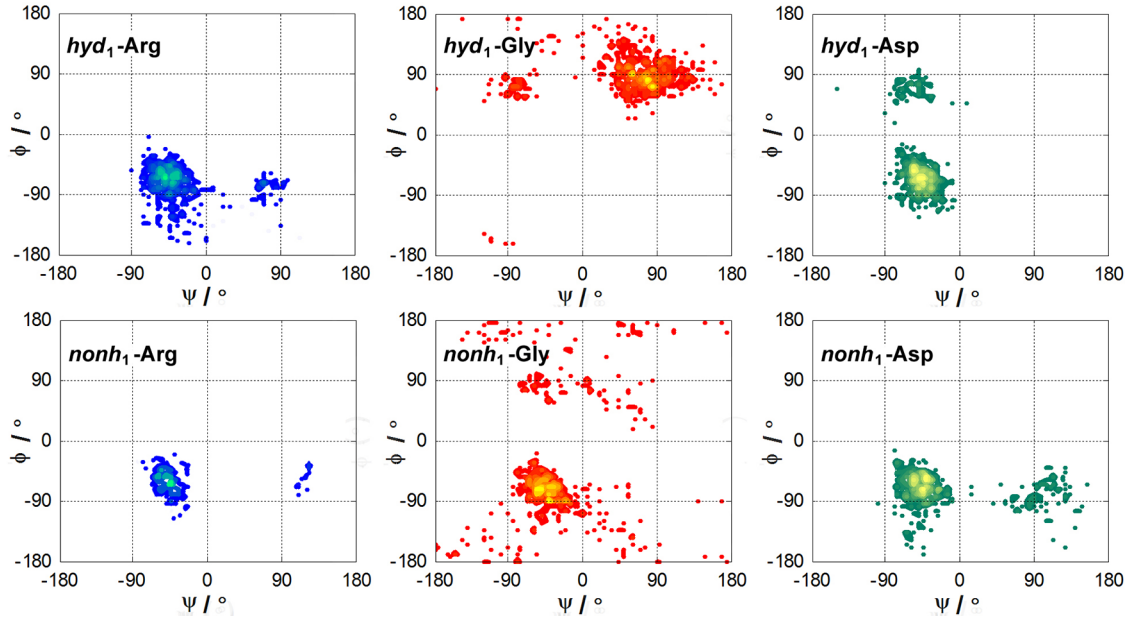

Figure 8. Distribution density of backbone dihedral pairs (Ψ, Φ) for RGD peptide mediated by an inner-sphere Ca^{2+} ion.

nonh-surfaces distribute in a similar way with the values approximating 0 when the *z*-distance is less than 4.0 Å. That is, both the hyd$_1$-O_{COO^-} and the nonh$_1$-O_{COO^-} atoms stay too far away from the rutile plane to form direct hydrogen bonds with the surface hydroxyls (see insets in Figure 6); however, there are two sharp peaks in the axial density curves (hyd-surface at ~5.2 and ~6.3 Å; nonh-surface at ~4.6 and ~5.0 Å), indicating that the Asp side chain is highly restrained by the hyd- or nonh-surface, even not involved in any H-bond connection with the surface hydroxyls, due to the presence of a mediating Ca^{2+} ion. The difference in the height of O_{COO^-} atoms (hyd$_1$-O_{COO^-} 4.6–7.0 Å; nonh$_1$-O_{COO^-} 4.0–6.0 Å) arises from the different binding configurations of the mediating cations after equilibration (hyd$_1$-Ca^{2+} TOTO; nonh$_1$-Ca^{2+} TD).

Figure 7 gives the 2D density maps of the adsorbed Ca^{2+} ions, and the functional atoms on the surface (threshold: 7 Å for hyd$_1$- and nonh$_1$-N_{NH_2} atoms; 7 Å for hyd$_1$-O_{COO^-} atoms; 6 Å for nonh$_1$-O_{COO^-} atoms). Different from the adsorbed Na^+ ion with a higher mobility in the *x*–*y* plane (see Figure 5), both TOTO mediating Ca^{2+} ion in the hyd$_1$-system and TD mediating Ca^{2+} ion in the nonh$_1$-system remain in the immediate vicinity of the COO^- group, appearing to be strongly bound to the surface, thereby inducing a "gluing" effect on the Asp residue. As a consequence, the negatively charged Asp side chain is anchored to the negatively charged hydroxylated/nonhydroxylated rutile (110) surface, indicated by the highly localized density of the O_{COO^-} atoms. This "gluing" effect agrees with the work performed by Monti et al.,[69] who drew the conclusion that Ca^{2+} ions were found to be practically locked in the interfacial region subsequent to their adsorption, acting as a bridge between the peptide and a negatively charged rutile (110), which was similar to the nonh-surface in this work. Moreover, the planar distribution of the hyd$_1$-N_{NH_2} atoms was also included into Figure 7a. The localized densities of hyd$_1$-N_{NH_2} and hyd$_1$-O_{COO^-} atoms indicate that the horseshoe configuration with both Arg and Asp side chains attached to the hyd-surface is preserved when mediated by an inner-sphere Ca^{2+} ion. On the contrary, the nonh$_1$-NH_2 groups, which are not shown in the 2D density map, stay farther away from the nonh-surface.

To reveal the conformational behavior of peptide backbone, the distribution density of backbone dihedral pairs (Ψ, Φ) (indicated by arrows in Figure 1c), which was not reported previously, will be shown in Figure 8. The dihedrals around the Arg and Asp residues do not vary dramatically on both hyd- and nonh-surfaces; however, the dihedrals around the glycine (Gly) residue, in the center of the peptide, disperse over a wider area for the nonh-surface than that for the hyd-surface. The

dx.doi.org/10.1021/am3031568 | ACS Appl. Mater. Interfaces 2013, 5, 2567–2579

horseshoe configuration contributes to restraining the structural change of the hyd_1-Gly backbone; however, the influence of intramolecular hydrogen bonds on the rigidity of the Gly backbone should not be simply denied, since the possibility of H-bond formation between the NH_2 groups and the COO^- group cannot be excluded according to their relative positions in the $x-y$ plane (Figure 7a). Hence, life periods of the available intramolecular hydrogen bonds during the final 2 ns production run were calculated, and the representative configurations of RGD on the hyd- and nonh-surfaces are shown in Figure 9. For the hyd_1-RGD (Figure 9a), one

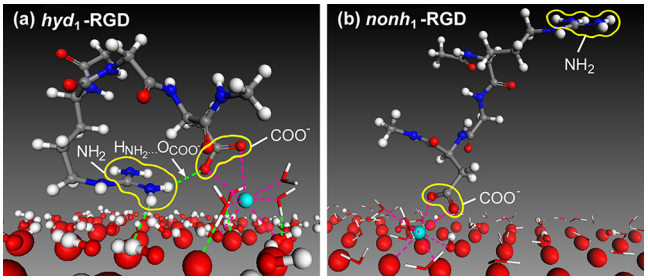

Figure 9. Representative configurations of RGD mediated by an inner-sphere Ca^{2+} ion: (a) hyd-surface, (b) nonh-surface. The bulk TiO_2 is omitted for clarity. The O_{BO} and O_{BOH} are shown in CPK representation, the TOH, H_{BOH}, RGD, and cations are shown in ball-and-stick representation, and the involved hydration water molecules are shown in stick representation. The hydrogen bonds and direct bonds (connected to the cations) are represented by green and magenta dashed lines, respectively.

hydrogen bond between the NH_2 group and the COO^- group ($H_{NH_2}\cdots O_{COO^-}$) exists for more than a third of the final 2 ns production run, facilitating the stability of the horseshoe configuration, thereby lessening the risk of significant structural changes of the peptide backbone. On the contrary, the $nonh_1$-RGD (Figure 9b) keeps one end of the molecule (COO^-) attached to the surface but the other end (NH_2) free to move in the solvent phase, thereby producing a flexible backbone.

A tightly packed Asp–rutile complex was presented on both hyd- and nonh-surfaces when mediated by an inner-sphere Ca^{2+} ion, even in the absence of hydrogen bonds between the peptide and the surface hydroxyls. Compared to the singly charged Na^+ ions, the doubly charged Ca^{2+} ions are more effective in bridging the negatively charged adsorbate to the negatively charged adsorbent, in agreement with many published experimental data.[70,71] Since a consensus of a clear molecular-level description of the rutile (110)–water interface has not been reached, there may be a mixed hydroxylation state in the real rutile (110) surface, as suggested in many literature works.[48,52,54,72] Thus, we may anticipate that the inner-sphere Ca^{2+} ions, capable of inducing a gluing effect on the COO^- group, will be actively involved in mediating the adsorption of negatively charged residues to the negatively charged rutile (110) surface in both hydroxylated and nonhydroxylated states. However, since the combined effect of Na^+ mediation and peptide–surface hydrogen bonds keeps the COO^- group staying on the hyd-surface, it is difficult for the Na^+ ions to trap the peptide on the rutile (110) surface in nonhydroxylated state, due to the small probability of H-bond formation between the peptide and the sparse surface hydroxyl groups on the surface.

Adsorption of RGD on the Negatively Charged Rutile Mediated by Outer-Sphere Ca^+. The outer-sphere binding configuration predominates in the Ca^{2+} ions adsorbed on the hyd- and nonh-surfaces (see Table 1); thus, the question must be asked whether the Ca^{2+} ion adsorbed at an outer-sphere binding site is capable of trapping the negatively charged Asp side chain to the negatively charged hydroxylated/non-hydroxylated rutile (110). To answer this question, extra simulations with a production run of 6 ns were performed for the above two surfaces, using different approaches to obtain the initial states of the testing assemblies. The initial configuration of the new hyd-system (denoted by "hyd_2-" below) derived from the final configuration of the hyd_1-system (t = 6 ns) by moving the RGD and the TOTO mediating Ca^{2+} ion farther away from the surface to allow the outer-sphere mediation of the peptide by the Ca^{2+} ion, with the original interaction between this specific cation and the peptide retained. One point needing to be clarified is that the outer-sphere mediating cations mentioned in this paper refer to the ones directly bound to the COO^- group but adsorbed on the surface as an outer-sphere species. For the new nonh-system (denoted by "$nonh_2$-" below), the initial state of the RGD–rutile complex was exactly the same as the $nonh_1$-system, except the distances from all the ions to the rutile plane were originally set to be larger than 8 Å (i.e., there is no preadsorbed Ca^{2+} ion in the vicinity of the COO^- group). The adsorption of RGD on the negatively charged hydroxylated rutile (110) mediated by an outer-sphere Ca^{2+} ion has been mentioned in our previous work very

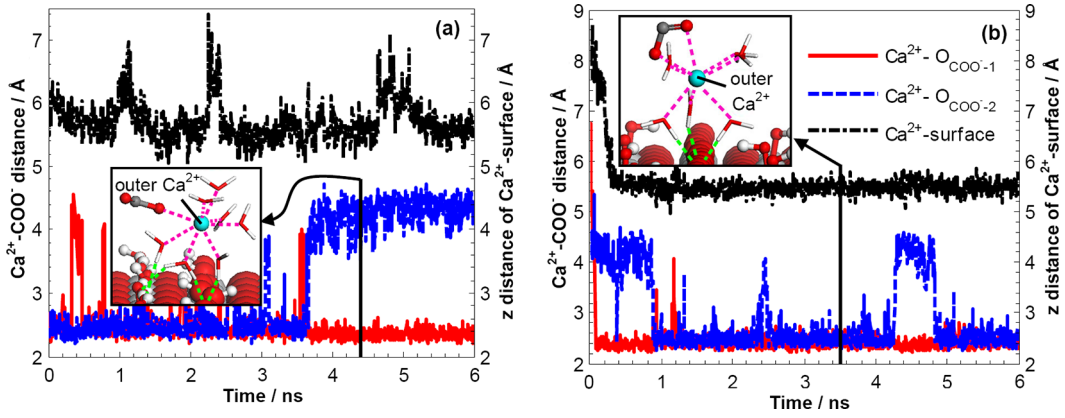

Figure 10. Evolution of distances from the outer-sphere mediating Ca^{2+} ion to the O_{COO^-} atoms, as well as z-position of this specific cation with respect to the rutile plane: (a) hyd-surface, (b) nonh-surface.

briefly;[56] therefore, extra detailed analysis of the hyd_2-system needs to be provided to compare with the results of the $nonh_2$-system.

To monitor the Asp/Ca^{2+}/rutile interaction, Figure 10 displays the evolution of distances from the special Ca^{2+} ion to the O_{COO^-} atoms, as well as its *z*-position with respect to the rutile plane (a: hyd-surface; b: nonh-surface). The outer-sphere Ca^{2+} cation in the hyd_2-system remains indirectly bound to the surface via the intermediate hydration waters (inset of Figure 10a), whereas in the $nonh_2$-system, a Ca^{2+} ion in the bulk phase approaches the COO^- group and the surface rapidly, adsorbing at an outer-sphere binding site (inset of Figure 10b). Moreover, only the $O_{COO^-}{}_{-1}$ atom remains coordinated to the mediating cation on the hyd-surface after t = 3.7 ns (Figure 10a), while the direct bond between the $O_{COO^-}{}_{-2}$ atom and the specific Ca^{2+} ion on the nonh-surface breaks and reforms during the final 2 ns production run (Figure 10b). To visualize the distribution of Arg and Asp side chains in the direction perpendicular to the rutile plane, the axial density profiles of O_{COO^-} and N_{NH_2} atoms for the new systems are plotted in Figure 11. The horseshoe configuration of RGD is found to be

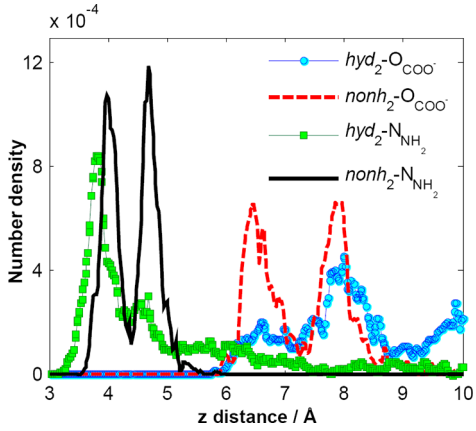

Figure 11. Axial density profile of functional atoms mediated by an outer-sphere Ca^{2+} ion on the hyd- and nonh-surfaces.

preserved in both hyd_2- and $nonh_2$-systems under the combined action of Arg−surface hydrogen bonds and the mediation of an outer-sphere Ca^{2+} ion.

The $nonh_2$-N_{NH_2} atoms keep a height of 3.5−5.5 Å from the rutile plane, forming stable hydrogen bonds with the nonh-surface, whereas the density of hyd_2-N_{NH_2} atoms distributes over the entire region (3 < *z*-distance < 10 Å) with a sharp peak centering at ∼3.80 Å, maintaining the H-bond connection with the hyd-surface during most of the simulation time. As discussed above, the Asp side chain mediated by an inner-sphere Ca^{2+} ion is highly restrained by the hydroxylated/nonhydroxylated rutile surface; however, when the COO^- group is bridged to the same surface by an outer-sphere mediating Ca^{2+} ion, the distances from the O_{COO^-} atoms to the rutile plane remain much larger and range more widely (height of hyd_1-O_{COO^-} vs height of hyd_2-O_{COO^-}: 4.6−7.0 Å vs 6.0−11.0 Å; height of $nonh_1$-O_{COO^-} vs height of $nonh_2$-O_{COO^-}: 4.0−6.0 vs 6.0−9.0 Å). That is, although the Ca^{2+} ion in an outer-sphere geometry is capable of bridging the peptide to the hyd-/nonsurface, the stability of Asp side chain in the direction perpendicular to the rutile plane is inferior to the one mediated by an inner-sphere Ca^{2+} ion.

The thresholds for obtaining the 2D density map of the adsorbed cations and the functional atoms on the surface (Figure 12) are selected as below: 6 Å for hyd_2- and $nonh_2$-N_{NH_2} atoms; 9 Å for hyd_2- and $nonh_2$-O_{COO^-} atoms. As we can see, the 2D densities of the mediating Ca^{2+} ion, Arg and Asp side chains in the hyd_2-system (Figure 12a) seem a little less localized than the corresponding items in the $nonh_2$-system (Figure 12b). Furthermore, both hyd_2-O_{COO^-} and $nonh_2$-O_{COO^-} atoms bound to an outer-sphere Ca^{2+} ion occupy a much larger binding domain in the *x*−*y* plane than that of hyd_1-O_{COO^-} or $nonh_1$-O_{COO^-} atoms mediated by an inner-sphere Ca^{2+} ion (Figure 7). Hence, it can be inferred that the binding mode of the mediating cation plays an important role in determining the mobility of the COO^- group. The inner-sphere mediating Ca^{2+} ion (see Figure 7) shows an extremely highly localized density, whereas the outer-sphere mediating Ca^{2+} ion (see insets of Figure 12) exhibits a higher mobility in the *x*−*y* plane. This is because the inner-sphere cation is partially dehydrated and directly binds to the surface hydroxyls or 1st H_2O molecules, which are nearly immobile on the surface. However, the outer-sphere cation keeps indirectly adsorbed at the interfacial region through its solvation shell, and the cation desolvation (the residence time of first coordination shell of water molecules around Ca^{2+} is 485 ps)[56] will result in a constant interruption and reformation of the Ca^{2+}−O_W bond network. Therefore, the locked inner-sphere Ca^{2+} ion induces a gluing effect on the Asp side chain, whereas the less stable Ca^{2+}−O_W connections produce a less localized outer-sphere mediating Ca^{2+} ion, resulting in a higher planar mobility of the COO^- group.

To estimate the structural stability of the peptide backbone, the distribution density of the backbone dihedral pairs is

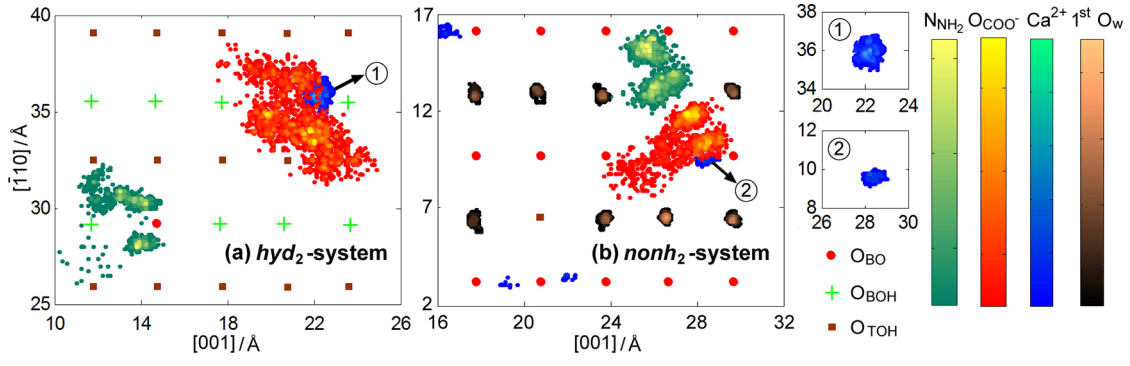

Figure 12. 2D density maps of functional atoms mediated by an outer-sphere Ca^{2+} ion: (a) hyd-surface, (b) nonh-surface.

dx.doi.org/10.1021/am3031568 | ACS Appl. Mater. Interfaces 2013, 5, 2567−2579

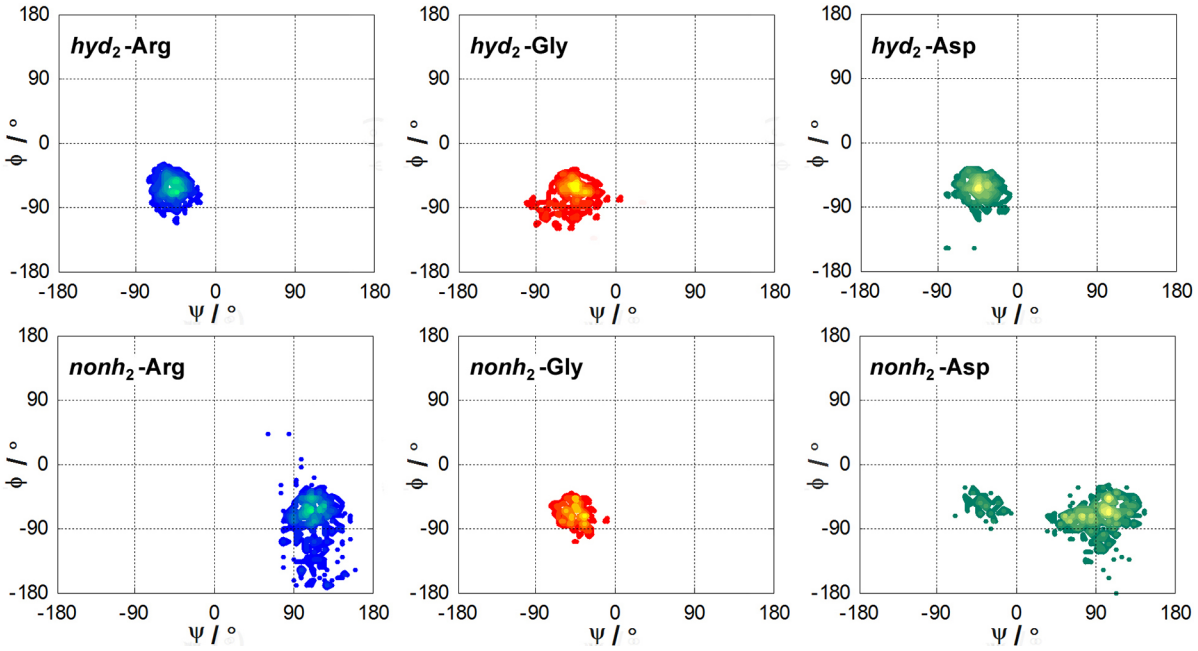

Figure 13. Distribution density of backbone dihedral pairs (Ψ, Φ) for RGD peptide mediated by an outer-sphere Ca^{2+} ion.

provided in Figure 13. The Gly dihedrals distribute in almost the same domain for the hyd_2- and $nonh_2$-systems (hyd_2-Gly Ψ: −105° to −10°, Φ: −120° to −35°; $nonh_2$-Gly Ψ: −75° to −10°, Φ: −115° to −40°); however, the dihedrals around the Arg and Asp residues vary slightly greater in the latter than that in the former. Since the horseshoe configuration is preserved in both systems, we speculate that some specific intramolecular interaction may give rise to the difference in the backbone dihedrals, and the representative configurations of RGD on the hyd- and nonh-surfaces were displayed in Figure 14. Different

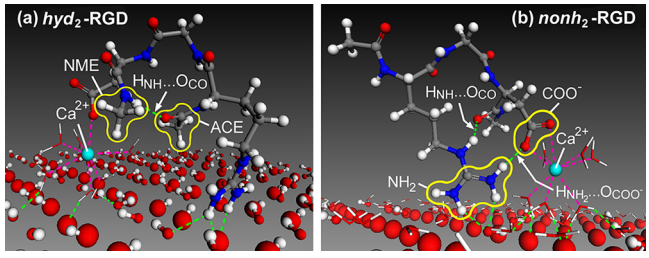

Figure 14. Representative configurations of RGD mediated by an outer-sphere Ca^{2+} ion: (a) hyd-surface, (b) nonh-surface. The bulk TiO_2 is omitted for clarity. The O_{BO} and O_{BOH} are shown in CPK representation, the TOH, H_{BOH}, RGD, and cations are shown in ball-and-stick representation, and the involved hydration water molecules are shown in stick representation. The hydrogen bonds and direct bonds (connected to the cations) are represented by green and magenta dashed lines, respectively.

from the hyd_1-RGD in Figure 9a, the distances from the hyd_2-NH_2 groups to the hyd_2-COO^- group are too large to form any hydrogen bond, as inferred from the 2D density map in Figure 12a; however, the spatial positions of the blocking groups make the intramolecular hydrogen bond still available in the hyd_2-system. As shown in Figure 14a, the ACE and NME blocking groups orientating toward the surface are kept together by the $H_{NH}\cdots O_{CO}$ hydrogen bond, which exists for more than half of the final 2 ns production run. In the $nonh_2$-system (Figure 14b), as expected, two intramolecular hydrogen bonds, i.e., $H_{NH}\cdots O_{CO}$ and $H_{NH_2}\cdots O_{COO^-}$, exist for more than 70% of the final 2 ns production run, holding the Arg and Asp residues together.

From the above, we can find that the rigidity of the Gly backbone is much higher in the hyd_2- and $nonh_2$-systems than that in the hyd_1-system, even sometimes the horseshoe configuration and the intramolecular hydrogen bonds coexist in these three systems. Two reasons may be responsible for it: (1) duration of intramolecular hydrogen bonds (hyd_1-system: ∼34%; hyd_2-system: ∼54%; $nonh_2$-system: ∼73% of the final 2 ns production run); (2) type of the intramolecular hydrogen bonds. In the hyd_1-system (Figure 9a), both the $H_{NH_2}\cdots O_{COO^-}$ hydrogen bond and the horseshoe configuration are involved in restraining the NH_2 groups and the COO^- group, thereby being regarded as one constraint. By contrast, the $H_{NH}\cdots O_{CO}$ hydrogen bond in the hyd_2-system (Figure 14a) acts on holding the ACE and NME blocking groups together, which should be classified into an extra constraint in addition to the horseshoe configuration. Also, two constraints coexist in the $nonh_2$-system (Figure 14b), i.e., the $H_{NH}\cdots O_{CO}$ hydrogen bond, and the $H_{NH_2}\cdots O_{COO^-}$ hydrogen bond in coordination with the horseshoe configuration. Moreover, the minor difference between the hyd_2- and $nonh_2$-systems in the densities of Arg and Asp dihedrals mentioned above should be attributed to the $H_{NH}\cdots O_{CO}$ hydrogen bond between the hyd_2-ACE and hyd_2-NME groups, which reduces the flexibility of the Arg and Asp backbones. Hence, it seems that the structural stability of RGD peptide bound to the negatively charged hydroxylated/nonhydroxylated rutile (110) surface in a horseshoe configuration can be facilitated by the intramolecular hydrogen bonds.

Overview of Interaction Energy. The RGD peptide detaches from the nonh-surface early even with a preadsorbed Na^+ ion, thus it is hard to directly compare the energetics data with when the peptide stays on the hyd-surface. However, for the systems with compensating Ca^{2+} ions, the RGD peptide

dx.doi.org/10.1021/am3031568 | ACS Appl. Mater. Interfaces 2013, 5, 2567−2579

Table 3. Interaction Energy for Different Group Pairs in the Systems with Ca^{2+} Ions (kcal·mol^{-1})

mediating cation		group pairs: RGD−rutile	Ca^{2+}−RGD[a]	Ca^{2+}−rutile[a]	sum
hyd-surface	outer-sphere Ca^{2+} (h_{ave} = 5.73)	−49.62 ± 4.14	−85.27 ± 4.15	−40.65 ± 4.67	−175.54
	inner-sphere Ca^{2+} (h_{ave} =3.88)	−20.81 ± 5.18	−110.59 ± 4.89	−160.67 ± 7.34	−292.07
nonh-surface	outer-sphere Ca^{2+} (h_{ave} =5.49)	−41.36 ± 2.29	−98.35 ± 4.81	−43.79 ± 3.23	−183.5
	inner-sphere Ca^{2+} (h_{ave} =3.08)	40.10 ± 3.52	−114.04 ± 4.65	−196.54 ± 5.62	−270.48

[a] Ca^{2+}−RGD and Ca^{2+}−rutile items refer to the interaction energies between the mediating Ca^{2+} ion and the RGD peptide, rutile surface.

adsorbs on both hydroxylated and nonhydroxylated rutile (110) surfaces, and its adsorption is the result of several contributions, involving mainly the mediation of an inner-/outer-sphere Ca^{2+} ion. This section was designed to provide a clear view of the mediating power of the Ca^{2+} ion and, therefore, the average interaction energy for different group pairs in each system was calculated for the trajectory of the final 2 ns production run (see Table 3).

The average heights (h_{ave}) of the mediating Ca^{2+} ions in the presented four systems are in the order: hyd_2-Ca^{2+} (outer-sphere) > $nonh_2$-Ca^{2+} (outer-sphere) > hyd_1-Ca^{2+} (inner-sphere) > $nonh_1$-Ca^{2+} (inner-sphere). From the data provided, we can find that the RGD−rutile interaction energy of the $nonh_1$-system with an inner-sphere Ca^{2+} ion is positive, while the value of the hyd_2-system with an outer-sphere Ca^{2+} ion is most negative. This may imply that the RGD in the $nonh_1$-system stays in an unfavorable position with respect to the surface. However, since the mediating Ca^{2+} ion interacts actively with both the peptide and the rutile surface, we should not focus exclusively on the RGD−rutile interaction; thus the interaction energies between the mediating Ca^{2+} ion and the peptide, rutile surface were also included in Table 3. The mediating Ca^{2+}-rutile interaction energy shows an opposite trend to the height of cation, that is, a higher mediating Ca^{2+} ion results in a lower interaction energy with the rutile surface. As emphasized before, both the inner- and outer-sphere mediating Ca^{2+} ions involved in this paper are directly bound to the COO^- group of Asp side chain, and consequently, the RGD-mediating Ca^{2+} interaction energy seems not to vary dramatically among the available systems, but the interaction energy between RGD and the inner-sphere mediating Ca^{2+} on the nonh-surface is the most negative, which may suggest that the peptide is favorably orientated with respect to the mediating cation.

The sum of interaction energies listed in Table 3 indicates a balance among the peptide, mediating cation, and surface. The trend of it is opposite to the height of cation, except that the value for the $nonh_1$-system is slightly less negative than the value for the hyd_1-surface, which may be attributed to the resulting conformations of the peptide that both Arg and Asp side chains keep attached to the hyd-surface (inner-sphere Ca^{2+}), whereas only the Asp side chain stays close to the nonh-surface (inner-sphere Ca^{2+}). Therefore, it can be concluded that although the $nonh_2$-RGD remains in a very unfavorable position with respect to the nonh-surface, the peptide is capable of keeping attached to the surface strongly within the sampling time as a result of the powerful mediation of an inner-sphere Ca^{2+} ion. This Ca^{2+} ion stays in the intermediate region, offsetting the unfavorable interaction between the peptide and the nonh-surface (40.10 ± 3.52 kcal·mol^{-1}), which can be inferred from the very negative values of the RGD-mediating Ca^{2+} interaction energy (−114.04 ± 4.65 kcal·mol^{-1}) and the mediating Ca^{2+}-rutile interaction energy (−196.54 ± 5.62 kcal·mol^{-1}).

CONCLUSIONS

Classical MD simulations have been employed to reveal the dynamical process of RGD adsorption on the negatively charged rutile (110) surfaces with two different hydroxylation states, in the presence of water and cations (Na^+ or Ca^{2+}). The simulation results indicate that the inherent nature of the cation determines its binding strength on both the negatively charged hydroxylated (hyd-) and the negatively charged nonhydroxylated (nonh-) surfaces, thereby affecting the adsorption propensity of RGD on the rutile (110).

In the NaCl solution, the negatively charged COO^- group is difficult to be trapped on the nonh-surface solely by the mediation of a preadsorbed Na^+ ion; thus the small probability of H-bond formation between RGD and the sparse hydroxyl groups induces an early desorption of the peptide. On the contrary, the mediating Na^+ ion on the hyd-surface is actively involved in trapping the COO^- group on the rutile (110), in coordination with the direct hydrogen bonds between the Asp side chain and the surface hydroxyl groups.

The doubly charged Ca^{2+} ions seem more effective than the singly charged Na^+ ions in bridging the negatively charged adsorbate to the negatively charged adsorbent, and the binding mode of the mediating Ca^{2+} ions plays an important role in determining the mobility of the COO^- group. The inner-sphere mediating Ca^{2+} ions are strongly bound to the interfacial region subsequent to their adsorption on both the hyd- and nonh-surfaces, thereby inducing a gluing effect on the Asp residue. This gluing effect results in the formation of a tightly packed RGD−rutile complex even in the absence of hydrogen bonds between the peptide and the surface. The powerful mediation of an inner-sphere Ca^{2+} ion has been confirmed by the interaction energy. Contrary to the locked inner-sphere Ca^{2+}, the outer-sphere mediating Ca^{2+} ions show a less localized density, thereby producing a higher mobility of the COO^- group, but the intramolecular hydrogen bonds help to restrain the conformational behavior of the backbone, facilitating the structural stability of RGD bound to both the hyd- and nonh-surfaces.

The findings presented indicate that there is a huge potential for introducing the microenvironment cues in order to tailor the specific protein−surface interactions. This approach, we anticipate, will blossom in the years to come, not in the least driven by the visionary, challenging, and important areas of nanoscale materials and bionano-assembly technologies.

ASSOCIATED CONTENT

Supporting Information

Charges of surface atoms for the negatively charged hydroxylated and nonhydroxylated rutile (110) surfaces (σ =

−0.208 C/m^2). Lennard-Jones parameters of SPC/E water, ions, and peptide atoms. Parameters of Buckingham potential for interaction between TiO_2 atoms and SPC/E water, peptide atoms. Parameters of Lennard-Jones potential for interaction between TiO_2 atoms and SPC/E water, peptide atoms. Validation of the force field and references. This material is available free of charge via the Internet at http://pubs.acs.org.

AUTHOR INFORMATION

Corresponding Author

*Fax: +86(0)451-86403252. E-mail: wuchunya1982@163.com (C.W.) chenmj@hit.edu.cn (M.C.).

Notes

The authors declare no competing financial interest.

ACKNOWLEDGMENTS

This work was supported by National Natural Science Foundation of China (No. 51201050) and the Research Fund for the Doctoral Program of Higher Education of China (No. 20102302110006). This research used resources of the National Energy Research Scientific Computing Center, which is supported by the Office of Science of the U.S. Department of Energy under Contract No. DE-AC02-05CH11231. P.T.C. and A.A.S. were supported by the U.S. Department of Energy (DOE), Office of Basic Energy Sciences, Geoscience Research Program, through Grant ERKCC72 to Oak Ridge National Laboratory, which is managed for DOE by UT Battelle, LLC under Contract No. DE-AC05-00OR22725.

REFERENCES

(1) Gray, J. J. *Curr. Opin. Struct. Biol.* **2004**, *14*, 110−114.
(2) Sarikaya, M.; Tamerler, C.; Jen, A. K. Y.; Schulten, K.; Baneyx, F. *Nat. Mater.* **2003**, *2*, 577−585.
(3) Latour, R. A. *Biointerphases* **2008**, *3*, FC2−FC12.
(4) Felice, R. D.; Corni, S. *J. Phys. Chem. Lett.* **2011**, *2*, 1510−1519.
(5) Petrie, T. A.; Raynor, J. E.; Reyes, C. D.; Burns, K. L.; Collard, D. M.; Garcia, A. J. *Biomaterials* **2008**, *29*, 2849−2857.
(6) Barber, T. A.; Ho, J. E.; De Ranieri, A.; Virdi, A. S.; Sumner, D. R.; Healy, K. E. *J. Biomed. Mater. Res. A* **2007**, *80A*, 306−320.
(7) Kilpadi, K. L.; Chang, P. L.; Bellis, S. L. *J. Biomed. Mater. Res.* **2001**, *57*, 258−267.
(8) Hennessy, K. M.; Pollot, B. E.; Clem, W. C.; Phipps, M. C.; Sawyer, A. A.; Culpepper, B. K.; Bellis, S. L. *Biomaterials* **2009**, *30*, 1898−1909.
(9) Vallee, A.; Humblot, V.; Pradier, C. M. *Acc. Chem. Res.* **2010**, *43*, 1297−1306.
(10) Costa, D.; Garrain, P. A.; Baaden, M. *J. Biomed. Mater. Res. A.* **2012**, *9999A*, 1−13.
(11) Tamerler, C.; Sarikaya, M. *Philos. Trans. R. Soc. A−Math. Phys. Eng. Sci.* **2009**, *367*, 1705−1726.
(12) Schneider, J.; Ciacchi, L. C. *J. Am. Chem. Soc.* **2012**, *134*, 2407−2413.
(13) Pierschbacher, M. D.; Ruoslahti, E. *Nature* **1984**, *309*, 30−33.
(14) Ruoslahti, E.; Pierschbacher, M. D. *Science* **1987**, *238*, 491−497.
(15) Brighton, C. T.; Albelda, S. M. *J. Orthop. Res.* **1992**, *10*, 766−773.
(16) Grzesik, W. J.; Robey, P. G. *J. Bone Miner. Res.* **1994**, *9*, 487−496.
(17) Ferris, D. M.; Moodie, G. D.; Dimond, P. M.; Gioranni, C. W. D.; Ehrlich, M. G.; Valentini, R. F. *Biomaterials* **1999**, *20*, 2323−2331.
(18) Nguyen, M. N.; Lebarbe, T.; Zouani, O. F.; Pichavant, L.; Durrieu, M. C.; Héroguez, V. *Biomacromolecules* **2012**, *13*, 896−904.
(19) Schliephake, H.; Scharnweber, D.; Dard, M.; Rossler, S.; Sewing, A.; Meyer, J.; Hoogestraat, D. *Clin. Oral Implant. Res.* **2002**, *13*, 312−319.
(20) Rammelta, S.; Illert, T.; Bierbaum, S.; Scharnweber, D.; Zwipp, H.; Schneiders, W. *Biomaterials* **2006**, *27*, 5561−5571.
(21) Chen, J.; Bly, R. A.; Saad, M. M.; AlKhodary, M. A.; El-Backly, R. M.; Cohen, D. J.; Kattamis, N.; Fatta, M. M.; Moore, W. A.; Arnold, C. B.; Marei, M. K.; Soboyejo, W. O. *Mater. Sci. Eng. C−Mater. Biol. Appl.* **2011**, *31*, 826−832.
(22) Maddikeri, R. R.; Tosatti, S.; Schuler, M.; Chessari, S.; Textor, M.; Richards, R. G.; Harris, L. G. *J. Biomed. Mater. Res. A.* **2008**, *84A*, 425−435.
(23) Schaffner, P.; Dard, M. *Cell. Mol. Life Sci.* **2003**, *60*, 119−132.
(24) Jones, F. H. *Surf. Sci. Rep.* **2001**, *42*, 79−205.
(25) Massaro, C.; Rotolo, P.; Riccardis, F. D.; Milella, E.; Napoli, A. *J. Mater. Sci.: Mater. Med.* **2002**, *13*, 535−549.
(26) Dachille, F.; Simons, P. Y.; Roy, R. *Am. Mineral.* **1968**, *53*, 1929−1939.
(27) Song, D. P.; Chen, M. J.; Liang, Y. C.; Bai, Q. S.; Chen, J. X.; Zheng, X. F. *Acta Biomater.* **2010**, *6*, 684−694.
(28) Zhang, H. P.; Lu, X.; Leng, Y.; Watari, F.; Weng, J.; Feng, B.; Qu, S. X. *J. Biomed. Mater. Res. A* **2011**, *96*, 466−476.
(29) Chen, M. J.; Wu, C. Y.; Song, D. P.; Li, K. *Phys. Chem. Chem. Phys.* **2010**, *12*, 406−415.
(30) Chen, M. J.; Wu, C. Y.; Song, D. P.; Dong, W. M.; Li, K. *J. Mater. Sci.: Mater. Med.* **2009**, *20*, 1931−1938.
(31) Monti, S.; Carravetta, V.; Zhang, W.; Yang, J. *J. Phys. Chem. C* **2007**, *111*, 7765−7771.
(32) Monti, S. *J. Phys. Chem. C* **2007**, *111*, 6086−6094.
(33) Wu, C. Y.; Chen, M. J.; Guo, C. Q.; Zhao, X.; Yuan, C. S. *J. Phys. Chem. B* **2010**, *114*, 4692−4701.
(34) Feng, B.; Weng, J.; Yang, B. C.; Chen, J. Y.; Zhao, J. Z.; He, L.; Qi, S. K.; Zhang, X. D. *Mater. Charact.* **2002**, *49*, 129−137.
(35) Lesins, V.; Ruckenstein, E. *Colloid Polym. Sci.* **1988**, *266*, 1187−1190.
(36) Ravichandran, S.; Madura, J. D.; Talbot, J. *J. Phys. Chem. B* **2001**, *105*, 3610−3613.
(37) Noinville, V.; Vidal-Madjar, C.; Sébille, B. *J. Phys. Chem.* **1995**, *99*, 1516−1522.
(38) Melander, W. R.; Elrassi, Z.; Horvath, C. *J. Chromatogr.* **1989**, *469*, 3−27.
(39) Imamura, K.; Kawasaki, Y.; Nagayasu, T.; Sakiyama, T.; Nakanishi, K. *J. Biosci. Bioeng.* **2007**, *103*, 7−12.
(40) Roddick-Lanzilotta, A. D.; McQuillan, A. J. *J. Colloid Interface Sci.* **1999**, *217*, 194−202.
(41) Rocha, S.; Pereira, M. C.; Coelho, M. A. N.; Möhwald, H.; Brezesinski, G. *Langmuir* **2007**, *23*, 5022−5028.
(42) Chen, H.; Su, X. D.; Neoh, K. G.; Choe, W. S. *Langmuir* **2008**, *24*, 6852−6857.
(43) Dishon, M.; Zohar, O.; Sivan, U. *Langmuir* **2009**, *25*, 2831−2836.
(44) Hugenschmidt, M. B.; Gamble, L.; Campbell, C. T. *Surf. Sci.* **1994**, *302*, 329−340.
(45) Henderson, M. A. *Surf. Sci.* **1996**, *355*, 151−166.
(46) Allegretti, F.; O'Brien, S.; Polcik, M.; Sayago, D. I.; Woodruff, D. P. *Phys. Rev. Lett.* **2005**, *95*, 226104.
(47) Brinkley, D.; Dietrich, M.; Engel, T.; Farrall, P.; Gantner, G.; Schafer, A.; Szuchmacher, A. *Surf. Sci.* **1998**, *395*, 292−306.
(48) Diebold, U. *Surf. Sci. Rep.* **2003**, *48*, 53−229.
(49) Goniakowski, J.; Gillan, M. J. *Surf. Sci.* **1996**, *350*, 145−158.
(50) Lindan, P. J. D.; Harrison, N. M.; Holender, J. M.; Gillan, M. J. *Chem. Phys. Lett.* **1996**, *261*, 246−252.
(51) Walle, L. E.; Borg, A.; Uvdal, P.; Sandell, A. *Phys. Rev. B* **2009**, *80*, 235436.
(52) Lindan, P. J. D.; Zhang, C. *Phys. Rev. B* **2005**, *72*, 075439.
(53) Zhang, W.; Yang, J.; Luo, Y.; Monti, S.; Carravetta, V. *J. Chem. Phys.* **2008**, *129*, 064703.
(54) Kowalski, P. M.; Meyer, B.; Marx, D. *Phys. Rev. B* **2009**, *79*, 115410.
(55) Ridley, M. K.; Machesky, M. L.; Palmer, D. A.; Wesolowski, D. J. *Colloids Surf. A* **2002**, *204*, 295−308.

(56) Wu, C. Y.; Skelton, A. A.; Chen, M. J.; Vlček, L.; Cummings, P. T. *Langmuir* **2012**, *28*, 2799−2811.
(57) Předota, M.; Vlček, L. *J. Phys. Chem. B* **2007**, *111*, 1245−1247.
(58) Předota, M.; Bandura, A. V.; Cummings, P. T.; Kubicki, J. D.; Wesolowski, D. J.; Chialvo, A. A.; Machesky, M. L. *J. Phys. Chem. B* **2004**, *108*, 12049−12060.
(59) Sano, K. I.; Shiba, K. *J. Am. Chem. Soc.* **2003**, *125*, 14234−14235.
(60) LAMMPS Molecular Dynamics Simulator Home Page. http://lammps.sandia.gov (accessed Jan 18, 2011).
(61) Cornell, W. D.; Cieplak, P.; Bayly, C. I.; Gould, I. R.; Merz, K. M., Jr; Ferguson, D. M.; Spellmeyer, D. C.; Fox, T.; Caldwell, J. W.; Kollman, P. A. *J. Am. Chem. Soc.* **1995**, *117*, 5179−5197.
(62) Berendsen, H. J. C.; Grigera, J. R.; Straatsma, T. P. *J. Phys. Chem.* **1987**, *91*, 6269−6271.
(63) Allen, M. P.; Tildesley, D. J. In *Computer Simulation of Liquids*; Oxford University Press Inc.: New York, 1989; p 22.
(64) Carravetta, V.; Monti, S. *J. Phys. Chem. B* **2006**, *110*, 6160−6169.
(65) Poly, F.; Chenu, C.; Simonet, P.; Rouiller, J.; Monrozier, L. J. *Langmuir* **2000**, *16*, 1233−1238.
(66) Libera, J. A.; Cheng, H.; Olvera de la Cruz, M.; Bedzyk, M. J. *J. Phys. Chem. B* **2005**, *109*, 23001−23007.
(67) Cheng, H.; Zhang, K.; Libera, J. A.; Olvera de la Cruz, M.; Bedzyk, M. J. *Biophys. J.* **2006**, *90*, 1164−1174.
(68) Wu, C. Y.; Skelton, A. A.; Chen, M. J.; Vlček, L.; Cummings, P. T. *J. Phys. Chem. C* **2011**, *115*, 22375−22386.
(69) Monti, S.; Alderighi, M.; Duce, C.; Solaro, R.; Tiné, M. R. *J. Phys. Chem. C* **2009**, *113*, 2433−2442.
(70) Thomson, N. H.; Kasas, S.; Smith, B.; Hansma, H. G.; Hansma, P. K. *Langmuir* **1996**, *12*, 5905−5908.
(71) Romanowski, G.; Lorenz, M. G.; Wackernagel, W. *Appl. Environ. Microbiol.* **1991**, *57*, 1057−1061.
(72) Zhang, C.; Lindan, P. J. D. *J. Chem. Phys.* **2003**, *118*, 4620−4630.